Bending Ultrathin Graphene at the Margins of Continuum Mechanics

D.-B. Zhang, E. Akatyeva, and T. Dumitrică

Phys. Rev. Lett. **106**, 255503 — Published 24 June 2011

DOI: 10.1103/PhysRevLett.106.255503

Bending ultra-thin graphene at the margins of continuum mechanics

D.-B. Zhang, E. Akatyeva, and T. Dumitrică

Department of Mechanical Engineering,

University of Minnesota, Minneapolis, MN 55455

Abstract

Deviations from continuum mechanics are always expected as structures scale down to nanoscale. We investigate the validity of the plate idealization of ultra-thin graphene by gaining insight into the response of chemical bonds to bending deformations. In the mono-layer, a bond orbital description of bending reveals the full breakdown of the plate phenomenology. In the multi-layer, objective molecular dynamics simulations directly identify the validity-margin and the role of discreteness in the plate idealization. Our result has implications for a broad class of phenomena where the mono-layer easily curves, and for the design of mass and force detection devices.

PACS numbers: 62.23.Kn, 62.25.-g, 62.20.D-

The recent identification of graphene structures with high degree of crystallinity [1], extraordinary high stiffness and strength [2], calls for an understanding of the applicability of classical continuum models in two dimensions (2D). In graphene the carbon atoms are disposed in a geometric structure that closely resembles the basal planes of bulk graphite. Because the usual surface relaxation effects [3] are absent, the in-plane elastic constants can be inferred directly from the well-studied [4] graphite. However, due to the discreteness in the number of layers N, the out-of-plane deformation modes, such as bending, are of a new nanomechanical nature. Plate idealizations are often used for practical investigations [5, 6]. Unfortunately, a validity-check of the plate phenomenology against the underlying microscopic behavior is missing. On the theoretical side, there are difficulties associated with such endeavor, indeed. A simple bending deformation breaks the translational symmetry on which the accurate quantum mechanical (QM) methods are relying on.

The well studied bulk graphite [4] offers a well-defined parameterization for the plate associated to an N-layer graphene: a Young's modulus of 1.02 TPa and a thickness of $h = NZ_0$, where $Z_0 = 3.35$ Å is the interlayer distance. It is well known that this model doesn't scale down to the mono-layer [7–9]. Indeed, based on the observation that a quadratic approximation to the tensional and bending energy of the mono-layer accurately describes the microscopic data [7], the second-derivatives of these dependences are interpreted as the elastic in-plane stiffness (C) and bending stiffness (D) parameters of the plate. They serve as input for the isotropic continuum relations $\mathrm{D} = \mathrm{Y}h^3/[12(1-\nu^2)]$ and $\mathrm{C} = \mathrm{Y}h$. Here ν is the Poisson ratio. Instead of giving the expected values, this approach leads to an unrealistically-high Young's modulus and a thickness even smaller than the diameter of one carbon atom, Table 1. In spite of the difficulties of defining the mono-layer thickness, the plate can be clearly parameterized by the bending and tension stiffnesses of graphene, and then used to model carbon nanotube assemblies under tension [8]. Because continuum mechanics is a phenomenology, the plate model has been long regarded as valid and useful. However, recent experimentation [10] in mono-layer graphene challenges this view since the measured out-of-plane resonant frequencies are not following the plate inverse-quadratic scaling with length. This suggests the plate idealization of the mono-layer is limited in scope, regardless of the way it is parameterized.

In this Letter we reveal that in the mono-layer, the severe deviation from the parameterization indicated by bulk originates in the breakdown of the plate phenomenology. This is due to the decoupling of bending and tensional deformations, as evidenced here by a bond orbital model

that relies on the extension into three dimensions of the $\sigma - \pi$ orbital separability [11, 12]. In the multi-layer, we witness the onset of the plate behavior and reveal the role of discreteness by direct microscopic simulations of the pure bending process. These simulations are possible only due to the recent theoretical advances involving objective molecular dynamics (MD) [13] and its coupling [14] with a realistic QM description of the interatomic interactions [density functional-based tight-binding (DFTB) [15, 16] extended [17] to capture the interlayer van der Waals (vdW) binding].

In the first part, we focus on the mono-layer and capture the essential physics behind the response of chemical bonds to arbitrary bending. To describe our theory based on the concept of bond orbitals [18], it is appropriate to begin with the well known partitioning of the wavefunction of hexagonal planar graphene in terms of orthogonal sp^2 hybrids pointing toward the nearest-neighbors, as well as p_z orbitals oriented perpendicular to the plane. Physically, the strong σ bonds formed by the overlap of the nearest neighbors sp^2 hybrids are responsible for the high in-plane stiffness C value shown in Table 1. The weak π bonds formed by the p_z orbitals, sometimes referred to as non-bonding [18], couple instead to the planar shape. Under a pure bending distortion of the mono-layer around an arbitrary axis, each carbon atom and its three nearest neighbors are no longer planar but located in the corners of a pyramid. This pyramidalization is accounted for using the π-orbital axis vector (POAV) construction [11]. The geometrical tilting of σ_i-bonds ($i = 1, 2, 3$) by an angle θ, Figure 1(a), is accomplished in POAV by introducing a degree of p_z atomic orbital mixing into the σ_i network. Note that to first order in curvature ($1/R$), the three tilting angles as well as bond lengths are common [12, 19]. Remarkably, the pyramidalization angle θ is sufficient for describing the curvature-induced shift in sp^2 hybridization. Under the orthogonality constraint, the π-states acquire a small s-orbital component

$$|h_\pi\rangle = \frac{1}{\sqrt{1+\lambda^2}}(|s\rangle + \lambda|p_z\rangle), \tag{1}$$

which alters the inversion symmetry, Fig. 1(a). Parameter λ depends solely on θ, as [11, 12] $\lambda = (1 - 3\sin^2\theta)/(2\sin^2\theta)$.

The POAV model does not capture the h_π misalignments, Fig. 1(b). To rationalize the relative orientation of the h_π-orbital axis vector and the h_π^i-orbital axis vector located in neighbor i, it is useful to note that in the bent layer, atoms are still equivalent. Relying on this objective symmetry and simple geometrical considerations, we obtained that the torsional angles φ_i made by the h_π^i

axis and the plane delineated by the h_π and σ_i axes satisfy to first order in $1/R$

$$\sum_{i=1}^{3} \varphi_i^2 = 24\theta^2. \tag{2}$$

Note also that inside the plane defined by the axes of σ_i and h_π, Fig. 1(b), the angle made by the projection of the h_π^i axis with the normal direction to the σ_i bond is θ.

The POAV framework offers an analytical approach to quantify the strain stored in the bent mono-layer. As such we find that the strain energy is dominated by the adjustment of the hopping integrals between the misaligned h_π hybrids. Indeed, a geometrical decomposition of the orbitals into *s*- and *p*-atomic orbitals oriented parallel and perpendicular to the interatomic separation, followed by a standard second-moment estimate of the bonding energy, yields the bending strain energy density (energy per atom divided by atomic area $S_0 = 2.71$ Å^2)

$$E_b \approx \sqrt{\sum_{i=1}^{3} \frac{\langle h_\pi^0 | H | h_\pi^i \rangle^2}{S_0^2}} - \frac{\sqrt{3}}{S_0} V_{pp\pi} = \frac{\sqrt{3}}{S_0}\left(2V_{ss\sigma} + 2\sqrt{2}V_{sp\sigma} - V_{pp\sigma} - 3V_{pp\pi}\right)\theta^2 - \frac{\sqrt{3}}{6S_0} V_{pp\pi} \sum_{i=1}^{3} \varphi_i^2. \tag{3}$$

The $\sqrt{3}$ factor reflects the celebrated resonance bonding correction [18]. More insight is obtained in the above expression by introducing the interatomic Hamiltonian matrix elements derived from Harrison's universal scaling rule [18] $V_{ss\sigma} = -4.99$ eV, $V_{sp\sigma} = 5.37$ eV, $V_{pp\sigma} = 8.39$ eV, and $V_{pp\pi} = -2.38$ eV. In the first term after the equal sign, the bond strengthening caused by the *s* presence in h_π cancels, within the error of the approximation, the in-plane geometrical misalignment of p_z orbitals. Thus, we focus on the second term in which the φ_i angles can be further related to θ with the help of the sum rule (2). Using the pyramidalization - curvature relation [12] $\theta = a_{\text{C-C}}/4R$, where $a_{\text{C-C}} = 1.42$ Å is the carbon-carbon equilibrium bond, one obtains

$$E_b'' \approx -\frac{2}{3} V_{pp\pi} = 1.6 \text{ eV}, \tag{4}$$

a microscopic expression in accord with the isotropic elastic attributes of the mono-layer. The good agreement with the DFTB data indicates that strain is largely due to the torsional misalignment between the neighboring POAVs.

What is important here is that the preceding bond orbital analysis reveals that the mono-layer doesn't behave as a plate since it exhibits a pure bending curvature without stretching and compressing its σ-network. A bent plate would involve extension (compression) on the convex (concave) sides, hence a coupling between D and C. This is why the earlier plate assumption based

on the D = $E_b^{"}$ interpretation led to the unphysical Y and h values showcased in the first line of Table 1. The demonstrated continuum breakdown in the mono-layer brings a natural question: What is the limit of applicability, in terms of N, for the isotropic plate?

In the second part, we approach the above question by carrying out DFTB simulations on a collection of N-layers graphene with $N = 2, ..., 9$, stacked in the Bernal pattern. In the flat case, the binding energy varied little with N, from 9.265 eV for $N = 1$ to 9.297 eV for $N = 5$, and the inter-layer spacing Z_0 was practically constant. Simulating a bending deformation poses a fundamental difficulty. Even when bent along the armchair direction, Fig. 2(a), the translational symmetry along the principal curvature is removed. This makes standard QM calculations adopting translational symmetry intractable. However, the uniformly bent mono-layer can be described with basic repetition rules involving translation operations with $\mathbf{T}$, and rotations of angle Ω performed around the bending axis. These operations are applied to a small objective motif, such as the $j = 1, ..., 4$ atoms of coordinates $\mathbf{X}_j$, Fig. 2(a). In each bent layer, the atomic coordinates in the cell indexed by integers ζ, η are

$$\mathbf{X}_{j,\zeta,\eta} = \eta\mathbf{T} + \mathbf{R}^{\zeta}\mathbf{X}_j, \quad j = 1, ..., 4. \tag{5}$$

The bending angle Ω of the rotational matrix $\mathbf{R}$ can take an arbitrary value. In the linear bending regime the structural parameters $\mathbf{T}$ and Ω are common for every layer.

The employed microscopic simulation method - objective MD [13] - is crucial in this investigation. Firstly, the introduced simplification in the number of atoms that are explicitly accounted for, enables QM relaxation calculations that otherwise would be beyond reach. In a bent N-layer graphene, eq. (5) represents the objective boundary conditions imposed over the $4N$ atoms, the analogous of the standard periodic boundary conditions of periodic MD. Thus, the method allows simulating the large scale linear bending process of both mono- and N-layered graphene by considering a minimum of $4N$ atoms. Secondly, the method allows us to impose pure bending, a condition of stress where only a bending moment is being applied. Because under the objective boundaries (5) the only constraint imposed on the simulation cell is Ω, the atomic positions are free to move away or toward the rotation axis of $\mathbf{R}$ and thus to relieve in-plane strains [20].

Fig. 2(c) illustrates the bending response of the bonds oriented along the principal curvature direction, on which the bending load is transferred most effectively. As expected, the equilibrium 1.42 Å value is maintained only in the bent mono-layer. For multi-layers, there is a splitting with N, indicating that the bent N-layer is stretched at some points and compressed at others, in agreement with the plate phenomenology. We even noted that the microscopic response can be described with

the assistance of the invariant neutral surface, on the opposite side of which there is extension and compression, Fig. 2(b). It is important to further note that through our boundary conditions (5), the curvature of bent graphene is not imposed but is the result of the relaxation [20]. The curvature of the neutral surface becomes a good definition for the curvature of the whole N-layer.

E_b maintains a quadratic dependence on $1/R$ for all N. The accumulation of in-plane strain becomes obvious in the separation with N of the strain energy curves (shown per atom) in Fig. 3(a). The strain stored in the mono-layer appears negligibly small even with respect to the bi-layer. Studying the energy differences between successive N-layered graphene at constant $1/R$, one concludes that there is an increased strain in the outermost and innermost layers as N grows. We infer that the main source of strain is the extension and compression of the constituent layers and that the $\mathrm{D} = E_{\mathrm{b}}^{"}$ interpretation is now justified. In mathematical terms, this means

$$E_b = \frac{1}{2}\mathrm{D}\left(\frac{1}{R}\right)^2 \approx \frac{1}{2(1-\nu^2)}\sum_{n=1}^{N}\mathrm{C}\varepsilon_n^2. \tag{6}$$

ε_n is the in-plane strain stored in the n^{th} layer. It was measured inside the objective domain, as the change in length along the principal curvature with respect to the $R\Omega$ length of the neutral line, Fig. 2(a). Expressing ε_n function of R and Z_0, gives [21]

$$\mathrm{D} \approx \frac{2\mathrm{C}Z_0^2}{1-\nu^2}\begin{cases}\sum_{n=1}^{N/2}(n-\frac{1}{2})^2, & N \text{ even}\\ \sum_{n=1}^{(N-1)/2} n^2, & N \text{ odd}\end{cases} = \frac{\mathrm{C}Z_0^2 N(N^2-1)}{12(1-\nu^2)}. \tag{7}$$

For $N \geq 2$, the D values predicted by eq. (7) using C=26.6 eV/Å are in agreement with those determined by second-order polynomial fits to the DFTB energy's dependence on $1/R$, Fig. 3(b) and Table 1, confirming the plate phenomenology.

The Y and h values obtained by using the plate relations and the DFTB computed $E_b^{''}$, Fig. 3(c) and (d) converge quickly to the bulk. The small deviations at small N are a signature of discreteness. Indeed, the effect can be captured analytically by noting the resemblance of eq. (7) with the standard thin-plate relation. One obtains

$$h = Z_0\sqrt{N^2-1} \quad \text{and} \quad \mathrm{Y} = \mathrm{C}N/h. \tag{8}$$

Thus, for $N \geq 2$ the N-layered graphene behaves with a $1/2N^2$ error, like a plate, parameterized by a C/Z_0 Young's modulus and a NZ_0 thickness. Interestingly, $h = 0$ obtained for $N = 1$ corresponds to the membrane without thickness model [10]. Then, the $D = 0$ value indicated by eq. (7) and entered in Table 1, shows the inability of this membrane to capture the QM POAV misalignment.

In conclusion, our QM microscopic investigation reveals that the bending strain in mono-layer and multi-layer graphene arises from different sources. The mono-layer can easily curve only by introducing a π-orbital misalignment between adjacent pairs of carbon atoms. The lack of σ-bond participation proves the breakdown of the plate phenomenology. This result has implications for a broad class of phenomena, where the graphene mono-layer bubbles [22], scrolls its edges [23], ripples [24], and twists [25] in spite of its enormous stiffness. In multi-layer, the vdW forces are mediating the load transfer between layers and bending involves extension or compression of the σ bonds. The plate phenomenology is now fulfilled. It was shown before [26] that the electronic structure also evolves with N, and approaches the graphite limit at $N = 10$. Here we obtained that the bulk plate model can be applied even at $N = 3$ with only a 6% error. Our result fully supports the plate treatment applied to multi-layer graphene in experiments [5, 6, 27] involving out-of-plane deformations without layer-sliding.

[1] K.S. Novoselov, et al., *Science* **306**, 666 (2004).

[2] C. Lee, et al., *Science* **321**, 385 (2008).

[3] M.P.J. Punkkinen, et al., *Phys. Rev. Lett.* **106**, 057202 (2011); Z.J. Wang, et al., *J. Appl. Phys.* **108** 083506 (2010).

[4] O.L. Blackslee, et al., *J. Appl. Phys.* **41**, 3373 (1970).

[5] D. Garcia-Sanchez, et al., *Nano Lett.* **8**, 1399 (2008).

[6] M. Poot, H.S.J. van der Zant, *Appl. Phys. Lett.* **92**, 063111 (2008).

[7] E. Hernandez, et al., *Phys. Rev. Lett.* **80**, 4502 (1998).

[8] Y. Huang, J. Wu, K.C. Huang, *Phys. Rev. B* **74**, 245413 (2006).

[9] O.A. Shenderova, V.V. Zhirnov, D.W. Brenner, *Crit. Rev. Solid State* **27**, 227 (2002).

[10] C.Y. Chen, et al., *Nature Nanotechnol.* **4**, 861 (2009).

[11] R.C. Haddon, *J. Am. Chem. Soc.* **108**, 2837 (1986); R.C. Haddon, *Science* **261**, 1545 (1993).

[12] T. Dumitrică, C.M. Landis, B.I Yakobson, *Chem. Phys. Lett.* **360**, 182 (2002).

[13] T. Dumitrică, R.D. James, *J. Mech. Phys. Solids* **55**, 2206 (2007).

[14] D.-B. Zhang, M. Hua, T. Dumitrică, *J. Chem. Phys.* **128**, 084104 (2008).

[15] D. Porezag, et al., *Phys. Rev. B* **51**, 12947 (1995).

[16] R. Rurali, E. Hernandez, *Comp. Mat. Sci.* **28**, 85 (2003).

[17] A. Carlson, T. Dumitrică, *Nanotechnol.* **18**, 065706 (2007).

[18] W.A. Harrison, Elementary Electronic Structure (World Scientific, 1999).

[19] This approximation was tested in carbon nanotubes, where the rolled-up construction is valid for radii larger than 0.8 nm.

[20] I. Nikiforov, et al., *Appl. Phys. Lett.* **96**, 123107 (2010).

[21] In materials exhibiting surface elastic constants and variable layer spacing [3], C and Z_0 should be taken n dependent.

[22] A.L.V. de Parga, et al., *Phys. Rev. Lett.* **100**, 056807 (2008).

[23] M.M. Fogler, A.H. Castro Neto, F. Guinea, *Phys. Rev. B* **81**, 161408(R) (2010).

[24] J.C. Meyer, et al., *Nature* **446**, 60 (2007).

[25] D.-B. Zhang, T. Dumitrică, *Small* **7**, 1023 (2011).

[26] B. Partoens, F.M. Peeters, *Phys. Rev. B* **74**, 075404 (2006).

[27] D.C. Wei, et al., *J. Am. Chem. Soc.* **131**, 11147 (2009).

FIG. 1: (color online) (a) Diagram showing the π-orbital in planar graphene and its change into h_π under bending. (b) Relative orientation of two h_π orbitals located on a carbon-carbon bond of bent graphene. The planes delineated by the σ_i bonds in (a) and by h_π and σ_i axes in (b) were hatched. The upwards arrows are the POAV.

FIG. 2: (color online) (a) A bent mono-layer in the armchair direction is composed of primitive motifs containing only four atoms. Neighboring motifs are generated by translating and rotating this motif along and around the OZ axis. (b) An $N = 3$ graphene bent with $\Omega = 3.6$ deg ($1/R = 0.15$ nm^{-1}), as obtained by objective MD relaxations. Dashed line is the neutral surface. (c) Length distribution of the carbon-carbon bonds oriented along the principal curvature, when $\Omega = 0.2$ deg.

FIG. 3: (color online) (a) DFTB bending strain energy as a function of curvature squared, from mono-layer to 5-layer graphene. (b) Second derivative of the bending energies extracted from the microscopic data, and D values (crosses) predicted by eq. (7). Plate model for graphene based on microscopic data: (c) Young's modulus and (d) thickness (normalized by N) as a function of N. The horizontal lines mark the C/Z_0 and Z_0 values.

TABLE I: The second derivative of the bending energy density with curvature, as computed from DFTB data, and the D values computed with eq. (7). The last two columns present the resulted plate model with a bending stiffness $E_b^{''}$, the in-plane stiffness C = 26.6 eV/Å^2, and Poisson ratio $\nu = 0.24$.

N	$E_b^{''}$ (eV)	D (eV)	Y (TPa)	h/N (Å)
1	1.6	0	5.2	0.82
2	162.7	158.4	1.40	2.98
3	660.3	633.5	1.27	3.26
4	1,589.1	1,583.8	1.26	3.29
5	3,206.7	3,167.6	1.24	3.31

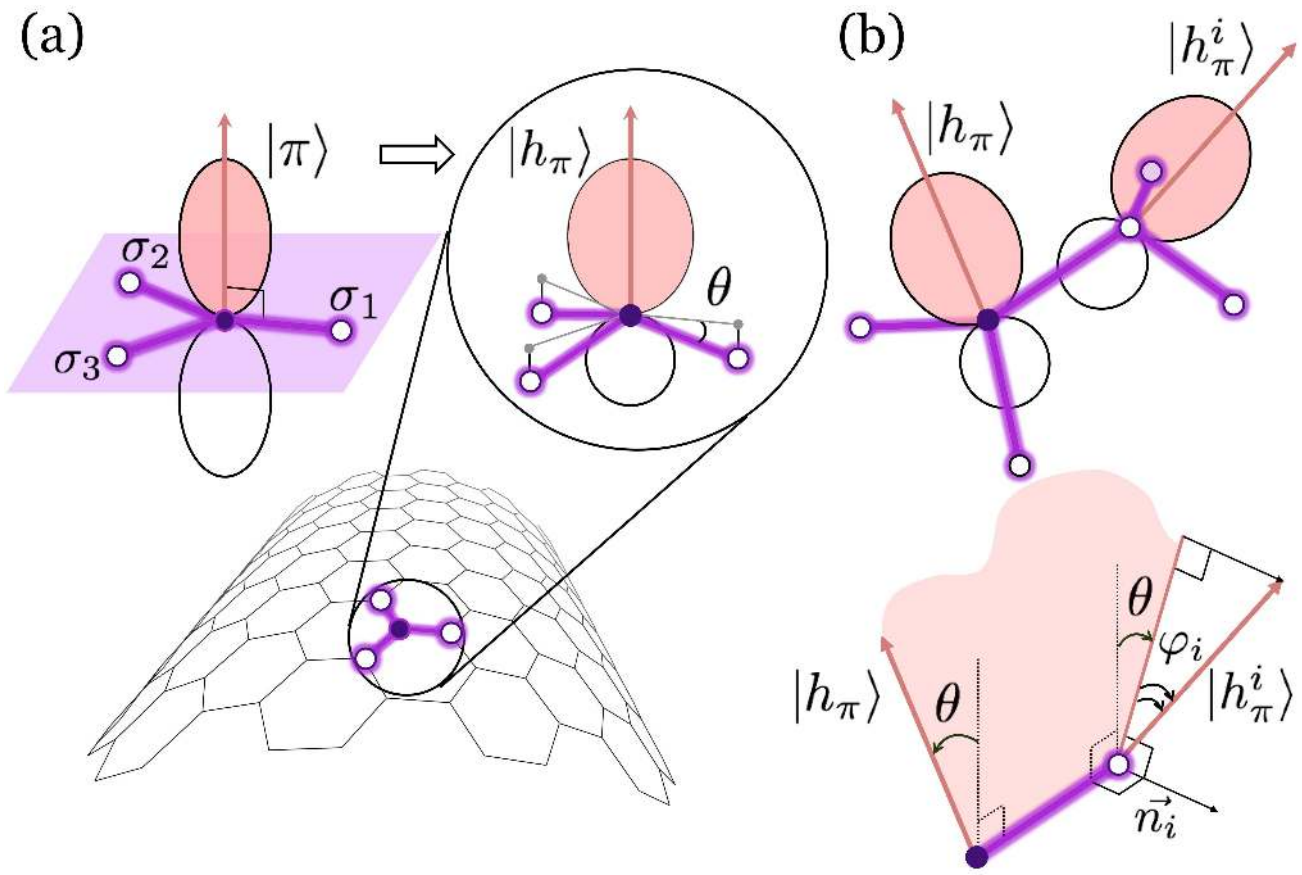

Figure 1 LD13547 25MAY11

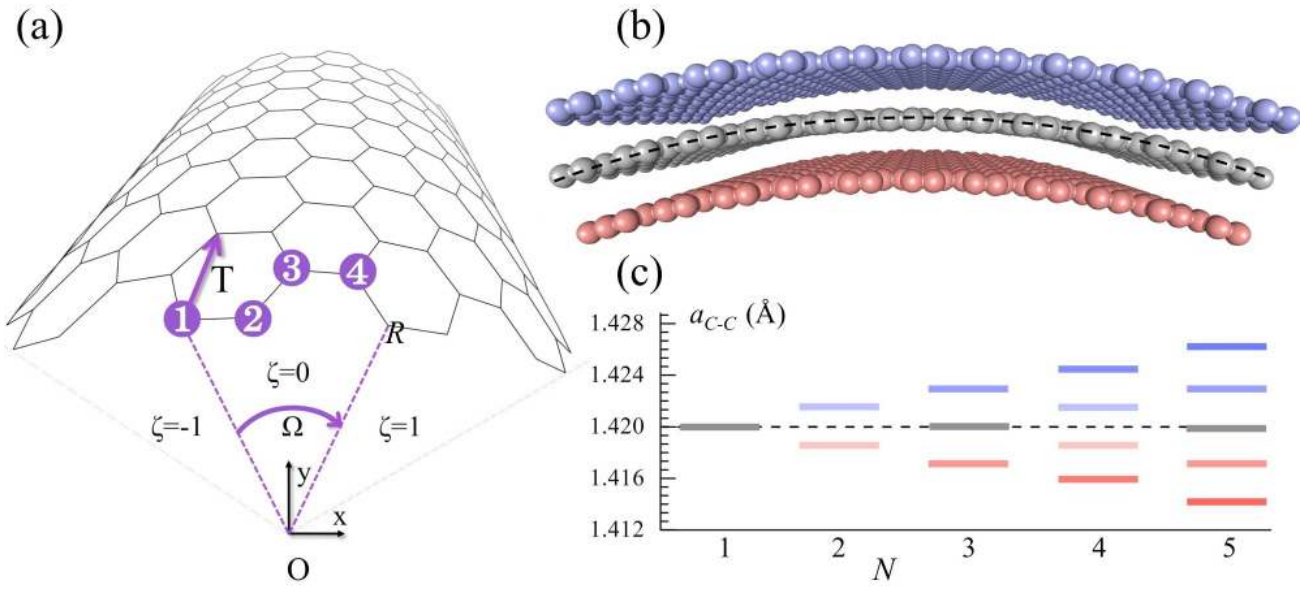

Figure 2 LD13547 25MAY11

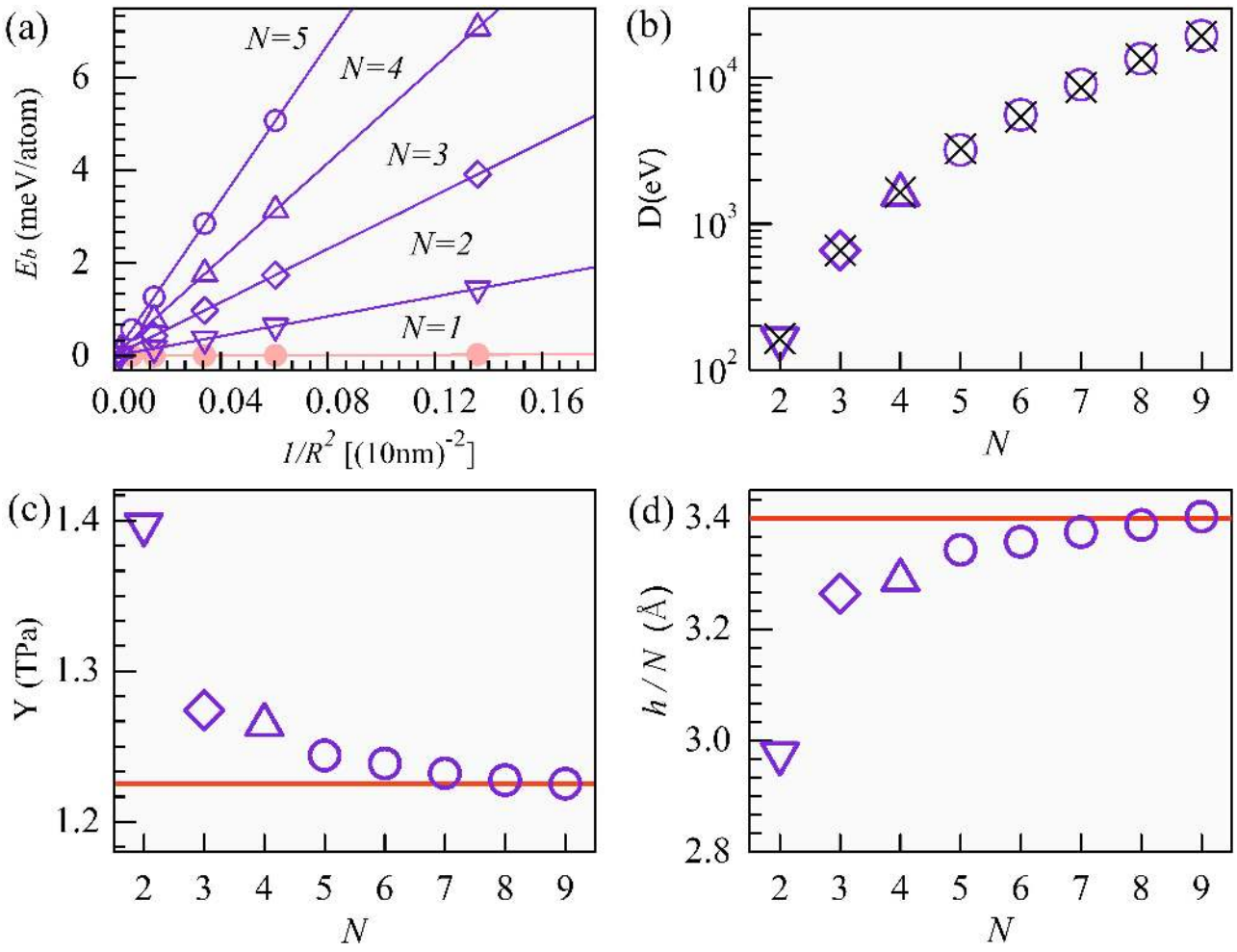

Figure 3 LD13547 25MAY11